informatics

MDPI

Article

GAMENet: Gender-Aware Morphology Encoder Network for Early Ischemia Heart Disease Classification

Deepti C * and Annapurna Dammur

Department of Computer Science and Engineering, Dayananda Sagar College of Engineering (Affiliated to Visveswaraya Technological University), Bengaluru 560078, India
* Correspondence: deeptic.cse@gmail.com

Abstract

Ischemic Heart Disease (IHD) is the leading cause of cardiovascular mortality worldwide. Early detection of ischemic changes using electrocardiogram (ECG) signals is vital for timely intervention and enhanced clinical outcomes. However, the diagnosis of IHD varies significantly between men and women. Women often present with atypical symptoms, and their cardiovascular risk is frequently underestimated, which leads to delayed diagnosis. Also, existing approaches face challenges in subtle early-stage abnormalities, single-lead ECG presentation, and the limited interpretability of deep learning models. These cause significant challenges to the accurate diagnosis of IHD. To address these, this study proposes a gender-aware framework, Gender-Aware Morphology Encoder Network (GAMENet), for early ischemic heart disease detection using 12-lead ECG signals with clinical metadata. A novel GAMENet is developed using the PTB-XL database. The Adaptive Morphology Deviation Encoder (AMDE) through Morphology Segment Extraction (MSEG-R) using R-Peak anchoring, isolates clinically relevant waveform components (P-wave, QRS complex, ST-segment, and T-wave) from the preprocessed ECG signals. The feature vector of morphology features is passed through dense layers with dropout regularization and a SoftMax classifier. Statistical and comparative analysis ensures that the proposed framework enables accurate IHD classification and improved interpretability.

Keywords: Adam optimizer; electrocardiogram; gender-aware framework; ischemic heart disease classification; R-peak anchoring

1. Introduction

Ischemic Heart Disease (IHD) is one of the leading causes of morbidity and mortality worldwide and remains a major public health concern due to its increasing prevalence and long-term cardiovascular complications [1,2]. According to the World Health Organization, IHD accounts for a substantial proportion of global deaths and imposes a socioeconomic burden on healthcare systems [3,4]. Hypertension, diabetes, dyslipidemia, obesity, and smoking are important problems in the development of IHD [5]. Increasing evidence shows there are substantial differences in the detection and treatment of IHD in women compared to men. The disparity in disease identification between men and women is still unaddressed. Women have a unique phenotype of IHD with less calcified lesions, higher prevalence of microvascular disease, and more nonobstructive plaques [6,7]. This ensures a need for the development of a gender-aware framework of IHD disease detection to efficiently detect IHD in both genders. Early identification and prevention of IHD is crucial in reducing the mortality rate of individuals with IHD. However, detecting IHD is a challenging problem

Check for updates

Academic Editor: Luc Bidaut

Received: 12 March 2026
Revised: 8 June 2026
Accepted: 14 June 2026
Published: 17 June 2026

Copyright: © 2026 by the authors. Licensee MDPI, Basel, Switzerland. This article is an open access article distributed under the terms and conditions of the Creative Commons Attribution (CC BY) license.

due to subtle electrocardiographic abnormalities in patient-specific cardiac morphology. Electrocardiography (ECG) is one of the most widely used non-invasive diagnostic tools for detecting myocardial ischemia and assessing cardiac abnormalities to provide real-time information about cardiac electrical activity [8–10]. Traditional single-lead ECG systems have been employed for myocardial infarction detection and long-term cardiac monitoring; however, their limited spatial information often restricts diagnostic sensitivity and specificity in complex ischemic conditions [11,12]. To overcome this, 12-lead ECG is utilized as a prognostic feature that efficiently predicts IHD diseases and cardiovascular diseases [13]. The Machine Learning (ML) approaches mainly focus on automated pattern identification that classifies illness units [14]. The advanced Deep Learning (DL) and Artificial Intelligence (AI) approaches include diverse phases of actions, such as preprocessing, feature extraction, and classification [15,16].

In recent years, Suhail and Razak [17] developed an automated diagnostic framework that detects cardiac diseases from ECG signals through Discrete Wavelet Transform (DWT) and Nonlinear Vector Decomposed Neural Network (NVDN) classifier. Iqbal [18] developed a DL-based model that combined AlexNet50 with fuzzy bi-clustering to detect subtle variations in ECG for cardiovascular disease detection. However, the model faced problems with a bias towards detecting classes. Majhi and Kashyap [19] proposed two tree-based explainer classifiers through Extreme Gradient Boosting (XGBoost) and Random Forest (RF) approaches for heart disease detection. The model utilized explainability to ensure transparency across medical professionals. However, the model faced noise problems in large ECG signals. To address this, Jyothi and Pradeepini [20] developed a Gaussian Kaiming Variance-based DL Neural Network (GKVDLNN) model for IHD detection. Rath et al. [21] analyzed four DL models, such as Radial Basis Function Network (RBFN), Restricted Boltzmann Machine (RBM), Autoencoder (AE), and the Self-Organizing Map (SOM), for IHD detection using ECG signals. Abdullayev et al. [22] developed an early detection AI-powered diagnostic framework that detects myocardial infarction from ECG. The framework developed a one-dimensional Convolutional Neural Network (CNN) for identifying ECG pattern characteristics. However, the model needed further improvements in generalizing the model through different ECG datasets. Her et al. [23] developed a framework for IHD using magnetocardiography that differentiates patients with stable IHD, acute coronary syndrome (ACS), and chest pain without cardiovascular disease.

The primary issues with existing works are that the current IHD detection approaches face challenges with insufficient sensitivity to subtle early ischemic changes. Especially, the major issue in current IHD diagnostics face challenges in the gender disparity between men and women. Clinical evidence indicates that women often present with atypical symptoms compared to men, and their cardiovascular risk is frequently underestimated, leading to delayed diagnosis. Male patients more frequently exhibit pronounced ST-segment elevation or depression, pathological Q-waves, and distinct infarction-related QRS abnormalities. In contrast, female patients often present with subtle ischemic ECG patterns, including diffuse ST-T abnormalities, T-wave inversion, microvascular ischemic changes, and non-specific repolarization disturbances. These differences make early diagnosis in women more challenging. Also, the use of single-lead ECG systems exhibits lower sensitivity in detecting ST-segment elevation, which is an important indicator of myocardial ischemia. Existing DL-based ECG analysis methods depend on end-to-end learning without extracting clinically relevant ECG morphological segments, such as P-wave, QRS complex, ST-segment, and T-wave. The absence of structured morphology-based feature extraction reduces interpretability and limits the model's ability to capture understated ischemic abnormalities. These limitations lack the accurate detection of ischemic heart disease across different patient demographics. The motivation of this study addresses the diagnostic

limitations associated with gender disparities, insufficient ECG sensitivity, and the lack of interpretable morphology-based analysis in existing IHD detection approaches. To overcome these challenges, this work proposes a Gender-Aware Morphology Encoder Network (GAMENet) that integrates ECG morphology analysis with patient demographic metadata. The proposed framework utilizes Adaptive Morphology Deviation Encoder (AMDE) through Morphology Segment Extraction using R-Peak anchoring (MSEG-R) to separate significant ECG waveforms, including the P-wave, QRS complex, ST-segment, and T-wave. These extracted features allow the model to capture subtle ischemic abnormalities. The proposed framework incorporates gender-aware metadata features, enabling the system to account for physiological variations in IHD presentation between men and women. The major contributions of the proposed work are summarized as follows:

- Proposed Gender-Aware Morphology Encoder Network (GAMENet): This study develops a novel gender-aware GAMENet framework for early IHD classification that integrates 12-lead ECG morphology features with patient metadata. This addresses gender-specific variations in ischemic presentation and enables IHD classification into normal, early ischemic, and severe ischemic MI.
- Morphology Feature Extraction using AMDE through MSEG-R: The study developed an AMDE to extract clinically significant ECG morphology features. The method employs MSEG-R to accurately separate key ECG waveform segments, including the P-wave, QRS complex, ST-segment, and T-wave. These enable the model to capture subtle ischemic abnormalities.
- Training Strategy using Adam with ReduceLROnPlateau scheduler: This study employs the Adam optimizer with the ReduceLROnPlateau learning rate scheduler to improve convergence stability and adaptive learning rate adjustment during training.

The remaining paper is structured as follows: Section 2 explains the background of the IHD and ECG signals, Section 3 describes the methodological part of the proposed GAMENet framework, Section 4 shows the experimental results, and Section 5 concludes the paper.

2. Background

Ischemic heart disease is also known as coronary artery disease. IHD arises due to the atherosclerotic obstruction of the coronary arteries or microvascular dysfunction [24]. IHD causes an unstable condition due to a severe atherothrombotic incident produced by plaque or blockage of coronary arteries, which accumulates within the intimal layer of the arterial wall. Plaque formation progresses in the coronary arteries, particularly the left anterior descending artery, right coronary artery, and left circumflex artery, which results in restricted blood flow. This decreases the supply of oxygen to the heart muscle. In early stages, ischemia is transient and reversible, presenting as mild electrical disturbances in the myocardium. However, if the obstruction becomes severe or a plaque ruptures, it can lead to permanent myocardial tissue damage [25,26].

The illustration of ischemic heart disease is depicted in Figure 1. ECG is one of the non-invasive diagnostic tools for monitoring the electrical activity of the heart. ECG signals are observed from the patient's arms, legs, and chest. ECG signals are generated by the depolarization and repolarization processes within cardiac muscle cells during each heartbeat. The ECG recording consists of 12 leads that show the electrical activity of various spatial orientations [27,28]. A 12-lead ECG is a diagnostic test that uses 10 electrodes. These electrodes record the heart's electrical activity from 12 different angles. The 12 leads are categorized as limb leads, augmented limb leads, and precordial leads. The limb leads (I, II, III) measure the differences between two electrodes. The augmented limb leads (aVR, aVL, aVF) are the unipolar leads. The precordial leads (V1, V2, V3, V4, V5, V6) provide

a horizontal plane. The ECG waveform includes morphological features, including the P-wave, QRS complex, ST-segment, and T-wave. The P-wave is the depolarization of the atria, and the QRS complex is the depolarization of the ventricles. Ventricular repolarization occurs as the T-wave. The ST-segment is positioned between the QRS complex and the T-wave. These are significant in the diagnosis of ischemic conditions. These abnormalities reflect basic physiological disturbances in the MI [29,30].

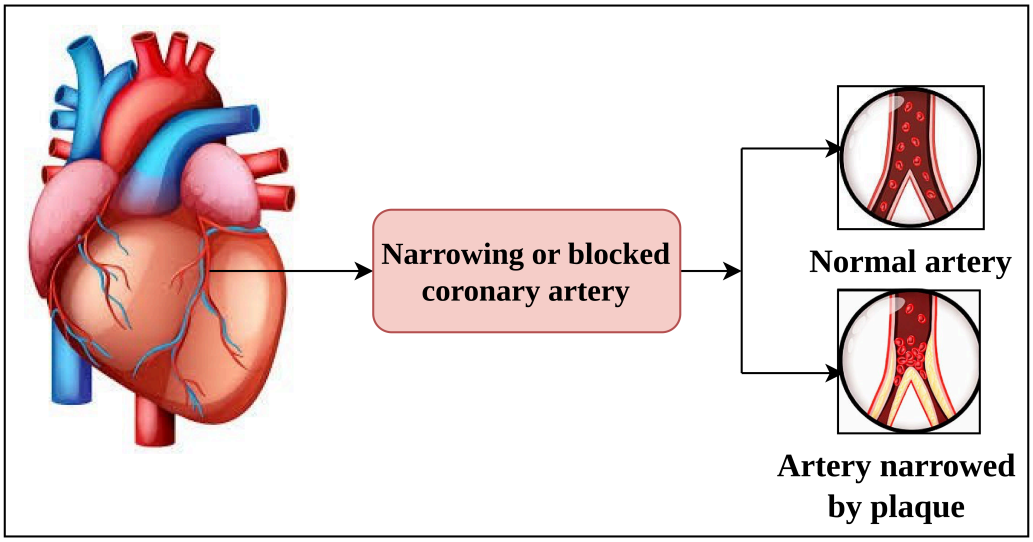


Figure 1. Illustrative diagram of the ischemic heart disease. Here arrows indicate the progression from the healthy heart to the development and assessment of coronary artery narrowing. The pink-colored box highlights the pathological condition (coronary artery narrowing or blockage), while the red regions in the artery illustrations represent blood flow and plaque accumulation. The upper image depicts a normal artery, whereas the lower image shows plaque-induced arterial narrowing associated with ischemic heart disease.

In this study, 12-lead ECG signals are utilized to detect early IHD. The ECG signals are obtained from the PTB-XL dataset [31], which provides annotated clinical ECG recordings along with demographic metadata. Metadata is the patient-related information that provides the contextual clinical details of the ECG signal. Each ECG signal follows a preprocessing step. This ensures consistent signal quality in ECG signals. The proposed approach focuses on segment-level morphology analysis, where important waveform regions are detected with the help of the R-Peak-anchored segmentation strategy. These segments are then analyzed using an AMDE, which computes deviation features to capture subtle waveform changes associated with ischemia. This enables the proposed framework to identify mild abnormalities in early-stage ischemia. ECG features are integrated with demographic metadata to enable gender-aware learning. This allows the system to account for variations in ischemic ECG presentation across different patient populations. ECG signals serve as the physiological input that enables the detection of ischemic abnormalities. This maintains clinical interpretability and computational efficiency in IHD classification.

3. Materials and Methods

The study develops a gender-aware GAMENet framework for early IHD detection, as illustrated in Figure 2. The study utilized the PTB-XL dataset from the PhysioNet that includes both ECG and metadata. The proposed GAMENet includes a dual-branch framework. Initially, the ECG signals and metadata are preprocessed using resampling, bandpass filtering, normalization, and fixed-length segmentation techniques. After preprocessing, the preprocessed data are fed to the Gender-Aware Morphology Encoder Network

(GAMENet). The proposed GAMENet contains two branches: the ECG feature extractor and the metadata feature extractor. In the first branch, AMDE captures subtle morphology deviations in ECG signals. Then, MSEG-R segments the ECG waveform into P-wave, QRS complex, ST-segment, and T-wave. Morphological deviations such as mean deviation, maximum deviation, slope deviation, and area deviation are computed for each segment. In the second branch, MLP generates a metadata feature representation. These two feature vectors are passed to a fusion layer using concatenation. The fused feature vector is passed through dense layers with dropout regularization and the SoftMax classifier. This categorizes the IHD into normal, early ischemic, or severe ischemic MI classes. This methodology addresses gender-specific variability in ischemic heart disease tasks.

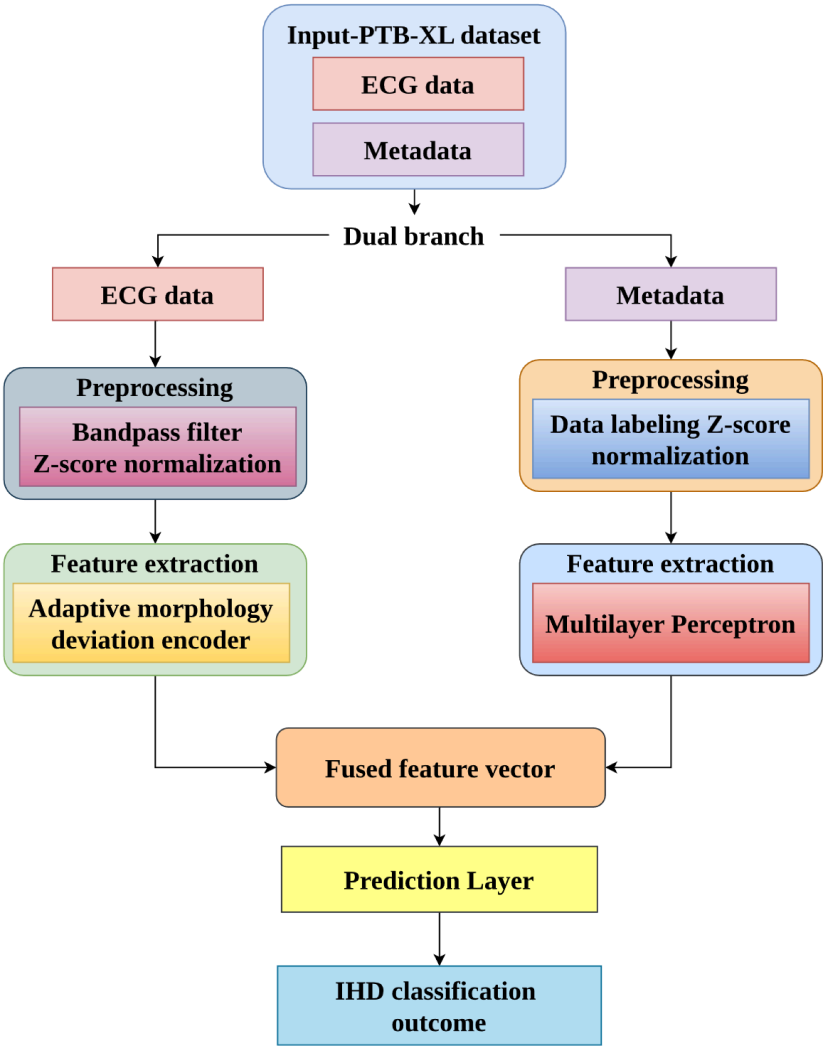


Figure 2. Schematic representation of the proposed gender-aware morphology encoder network for ischemic heart disease classification. Arrows indicate the flow of information through the proposed dual-branch architecture and the color-coded blocks represent different processing stages. The two branches independently learn complementary representations from ECG signals and metadata before being fused into a unified feature vector for IHD classification.

3.1. Dataset Description

The study utilized the PTB-XL database that includes both ECG data and metadata. The PTB-XL database includes a 12-lead ECG clinical data of unprecedented size. It includes 21,837 clinical 12-lead ECG records from 18,885 patients of 10 s in length. These records were sampled at 500 Hz and 100 Hz with 16-bit resolution, as illustrated in Table 1. The dataset

includes 71 different types of heart diseases with five major classes. Each 12-lead ECG recording consists of the cardiac electrical activity information essential for ischemia analysis.

Table 1. Number of individual classes in the PTB-XL dataset.

Class	Description	Number of Records
NORM	Normal ECG	9514
CD	Conduction Disturbance	4898
STTC	ST/T Change	5235
MI	Myocardial Infarction	5469
HYP	Hypertrophy	2649

The ECG records of PTB-XL are accompanied by metadata, including demographic attributes, diagnostic superclass annotations, and ECG measurement information. In this study, only the demographic variables age and sex were used as predictor metadata inputs to the proposed GAMENet framework. The diagnostic superclass annotations were utilized for label generation and dataset restructuring, while ECG interpretation statements and measurement annotations were not included as model input features to avoid information leakage. The PTB-XL dataset contains five major diagnostic classes, including Normal ECG (NORM), Myocardial Infarction (MI), ST/T Change (STTC), Conduction Disturbance (CD), and Hypertrophy (HYP). In this study, these diagnostic labels were reorganized into three clinically relevant categories for ischemia-focused classification. Specifically, records labeled as NORM were assigned to the "Normal" category. Records associated with STTC were grouped into the "Early Ischemic Heart Disease" category because ST-segment and T-wave abnormalities are clinically associated with early ischemic and repolarization disturbances. Records labeled as MI were assigned to the "Severe Ischemic MI" category to represent advanced ischemic myocardial injury. The CD and HYP classes were excluded from the final classification framework because these conditions may introduce non-ischemic ECG abnormalities that could confuse ischemia-specific morphology learning. This restructuring strategy enabled the proposed framework to focus specifically on ischemic progression patterns while maintaining clinically meaningful label definitions. This facilitates the development of a gender-aware ischemia detection framework.

3.2. Preprocessing

The preprocessing phase includes two parallel pipelines: ECG signal preprocessing and metadata preprocessing. The preprocessing phase enhances the quality of the dataset by ensuring data consistency and reducing noise, which supports the proposed GAMENet for ischemia classification.

3.2.1. ECG Data Preprocessing

In this phase, 12-lead ECG records are first loaded using the Waveform Database (WFDM) toolkit [32]. ECG signals in the dataset include varying sampling frequencies. These recordings are resampled to a sampling rate of 100 Hz to ensure temporal consistency across samples. Then, a bandpass filter [33] filters the signals from 0.5 to 40 Hz to eliminate noise and baseline artifacts in the dataset.

The reduced cutoff frequency (0.5 Hz) eliminates the respiratory and motion artifact baseline wander, as shown in Figure 3. The high-frequency noise is eliminated by the upper cutoff frequency (40 Hz). The filtered signal $F_s(x)$ is represented in Equation (1):

$$F_s(x) = Bf_{0.5-40HZ}\{F(x)\} \quad (1)$$

where $F(x)$ denotes the raw ECG signal and Bf represents the bandpass filtering operation. Then, Z-score normalization [34] is applied to standardize the amplitude variations and stable model training, as denoted in Equation (2):

$$Z_{norm}(x) = \frac{F_s(x) - \varphi}{\alpha} \quad (2)$$

where φ and α denote the mean and standard deviation of the filtered signal, respectively. Each ECG recording is trimmed to a fixed length of 1000 samples per lead to maintain a uniform input dimension. This results in a standardized matrix of size 1000×12.

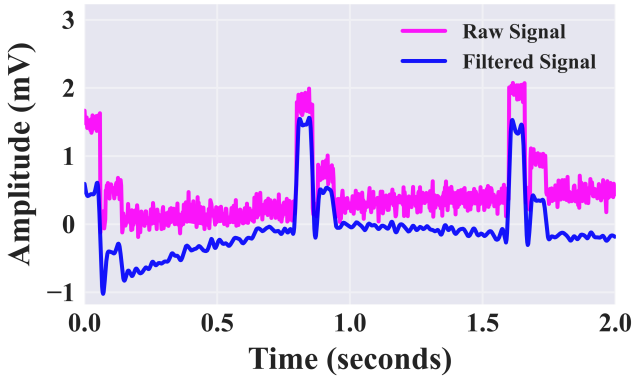


Figure 3. Visualization of the filtered ECG signal through bandpass filtering.

3.2.2. Metadata Preprocessing

This phase preprocesses the demographic metadata obtained from the PTB-XL dataset. The proposed framework utilizes the non-diagnostic demographic variables, specifically age and sex, as metadata predictors. The categorical sex attribute was converted into binary numerical representation using label encoding [35]. The age attribute was standardized using Z-score normalization to maintain consistent feature scaling during training. Z-score normalization standardizes its scale and prevents dominance over other features during training. This leads to efficient feature extraction and classification for IHD.

3.3. Gender-Aware Morphology Encoder Network

The proposed GAMENet is designed as a dual-branch architecture that extracts interpretable ECG morphology features and integrates demographic metadata for personalized IHD classification.

Branch 1: ECG Feature Extraction through Adaptive Morphology Deviation Encoder.

In this study, the feature extraction process captures the clinically important morphology deviations associated with IHD. We utilize the Adaptive Morphology Deviation Encoder (AMDE) to capture subtle morphology deviations in ECG signals, as shown in Figure 4. The AMDE module is introduced to learn a compact latent representation that preserves clinically meaningful morphology characteristics while enhancing feature interaction modeling and discriminative capability for IHD classification. The preprocessed 12-lead ECG signal (Y) is denoted as $Y \in \mathbb{R}^{T*12}$, where $T = 1000$ denotes the number of time samples and 12 represents the leads. Initially, the moving average method [36] is utilized to compute the smooth baselines of an ECG signal. It extracts the baseline wander from the raw ECG signals. Although morphology deviation features are explicitly extracted from ECG waveform regions, these handcrafted descriptors remain high-dimensional and exhibit strong inter-feature correlations across ECG leads and morphology segments. The proposed encoder network learns compact latent feature representations that preserve clinically relevant morphology information while reducing redundancy and improving class

separability. The encoder additionally enables effective fusion between ECG morphology descriptors and demographic metadata, allowing the framework to model sex-specific ischemic ECG variations more effectively than direct feature-based classification. For each lead ($l = 1, 2, \ldots, 12$), the baseline signal $B_l(x)$ is calculated, as denoted in Equation (3):

$$B_l(x) = \frac{1}{W} \sum_{j=x-\frac{W}{2}}^{x+\frac{W}{2}} Y_l(j) \tag{3}$$

where W represents the window size of the moving average filter and x represents the sample index within the segment. $Y_l(j)$ represents the amplitude of the preprocessed ECG signal at sample index j. After baseline estimation, we introduce a Morphology Segment Extraction using R-Peak anchoring (MSEG-R) [37]. R-peaks (R_w) are detected as stable temporal landmarks in the ECG signal. MSEG-R extracts clinically relevant ECG morphology regions, including the P-wave region, QRS complex, ST-segment region, and T-wave region. For each segment $E_{l,s}(x)$, the morphology deviation is computed by subtracting the estimated baseline $B_l(x)$ from the segment, as represented in Equation (4):

$$D_{l,s}(x) = E_{l,s}(x) - B_l(x) \tag{4}$$

where $D_{l,s}(x)$ denotes the morphology deviation signal for lead l and segment type $s \in \{P, QRS, ST, T\}$. $B_l(x)$ represents the moving-average baseline estimated for lead l. From Equation (4), we calculated four discriminative statistical features to capture morphological abnormalities. In the proposed framework, the detected R-Peak serves as a temporal anchor for heartbeat alignment. Following R-Peak localization, morphology regions were approximated using predefined temporal windows relative to the R-Peak position. The QRS complex region was centered around the detected R-Peak, while preceding and succeeding temporal windows were utilized to isolate the P-wave region, ST-segment region, and T-wave region, respectively. This strategy enabled consistent extraction of clinically relevant ECG morphology regions across cardiac cycles. The proposed method focuses on morphology-region extraction for feature learning. Statistical morphology deviation features, including mean deviation, maximum deviation, slope deviation, and area deviation, were subsequently computed from each extracted morphology region.

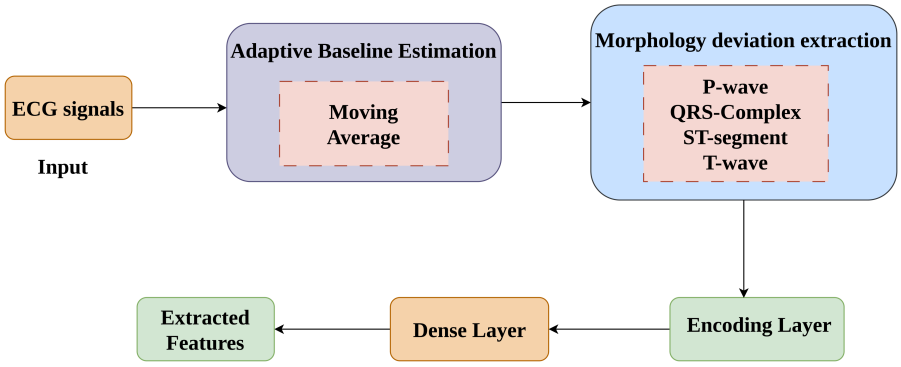


Figure 4. Architecture diagram of the proposed AMDE for feature extraction. ECG signals are first processed using adaptive baseline estimation with a moving average filter, followed by morphology deviation extraction of the P, QRS, ST, and T segments. The extracted information is encoded and passed through a dense layer to obtain discriminative features. Black arrows indicate the direction of data flow between processing stages and the color-coded blocks represent different functional modules.

The mean deviation measures the average displacement of the segment from the baseline, as denoted in Equation (5):

$$g_{mean}^{l,s} = \frac{1}{N}\sum_{x=1}^{N} B_{l,s}(x) \tag{5}$$

Then, the maximum deviation captures the largest abnormal deviation magnitude, as expressed in Equation (6):

$$g_{max}^{l,s} = max\left|B_{l,s}(x)\right| \tag{6}$$

The slope deviation captures the rate of change across the segment, as represented in Equation (7):

$$g_{slope}^{l,s} = \frac{B_{l,s}(x_{end}) - B_{l,s}(x_{start})}{x_{end} - x_{start}} \tag{7}$$

The area deviation measures the cumulative deviation over the segment duration, as mentioned in Equation (8):

$$g_{slope}^{l,s} = \sum_{x=1}^{N} B_{l,s}(x) \tag{8}$$

These features capture subtle ST-segment elevation, T-wave abnormalities, and other ischemic morphology variations. The extracted morphology features are also clinically relevant for modeling sex-specific ischemic presentations. In male patients, ischemic abnormalities are often associated with stronger ST-segment deviation patterns and pronounced QRS morphology alterations. Female patients exhibit comparatively subtle ST-T changes, flattened or inverted T-waves, and non-specific repolarization abnormalities associated with microvascular ischemia. Extracting waveform-specific deviation features from the P-wave, QRS complex, ST-segment, and T-wave regions, the proposed GAMENet framework is capable of learning these gender-dependent variations. The deviating features extracted from all segments across all 12 leads are concatenated to form a feature vector (C_{ECG}), as expressed in Equation (9):

$$C_{ECG} = [g_1, g_2, \ldots, g_n] \tag{9}$$

where g_i represents the feature vector corresponding to the i-th segmented waveform instance. Finally, this feature vector is passed through an encoding layer implemented as a fully connected dense layer to obtain an ECG representation, as expressed in Equation (10):

$$Z_{ECG} = \alpha(W_d C_{ECG} + B_d) \tag{10}$$

where Z_{ECG} represents the resulting encoded vector. The W_d and B_d denote the learnable weights and bias of the dense layer and α represents the nonlinear activation function. These extracted features are fused with metadata features for IHD classification.

Branch 2: Metadata Feature Extraction through Multilayer Perceptron.

In this phase, the input metadata vector M is passed through a Multilayer Perceptron (MLP) [38] to learn nonlinear demographic patterns associated with ischemic risk. MLP architecture is shown in Figure 5. MLP incorporates three layers: input layer, hidden layer, and output layer. The input layer includes the raw metadata feature vector values. The hidden layer units are selected based on initial experiments. The output layer utilizes the SoftMax activation function. The MLP formation is expressed as in Equation (11):

$$Z_{meta} = \vartheta(W_m M + B_m) \tag{11}$$

where W_m signifies the learnable weight matrix and B_m denotes the bias vector. ϑ represents the activation function. These represent the learned metadata feature representation which

captures gender-specific differences in IHD disease. After extracting the ECG features (Z_{ECG}) from the AMDE and the metadata features (Z_{meta}) from the MLP, the representations are combined in the fusion layer F. The representations are fused using concatenation, as denoted in Equation (12):

$$F = [Z_{ECG}||Z_{meta}] \tag{12}$$

where $||$ represents the concatenation operation. This allows the model to learn relationships between ECG patterns and demographic attributes. The fused representation is fed through a fully connected dense layer with dropout regularization, as expressed in Equation (13):

$$Z_{prediction} = dropout(\rho(W_p F + B_p)) \tag{13}$$

where W_p and B_p denote the learnable parameters and ρ represents the Rectified Linear Unit (ReLU) activation function. Then, the SoftMax layer is employed to estimate the probability distribution over the diagnostic classes: normal, early ischemic, and severe ischemic MI. The SoftMax function is expressed in Equation (14):

$$Z_u = \frac{e^{z_u}}{\sum_{v=1}^{3} e^{z_v}} \tag{14}$$

where Z_u denotes the predicted probability for class u. z_u and z_v represent the corresponding logit before normalization. This enables gender-aware IHD classification while maintaining interpretability and computational efficiency.

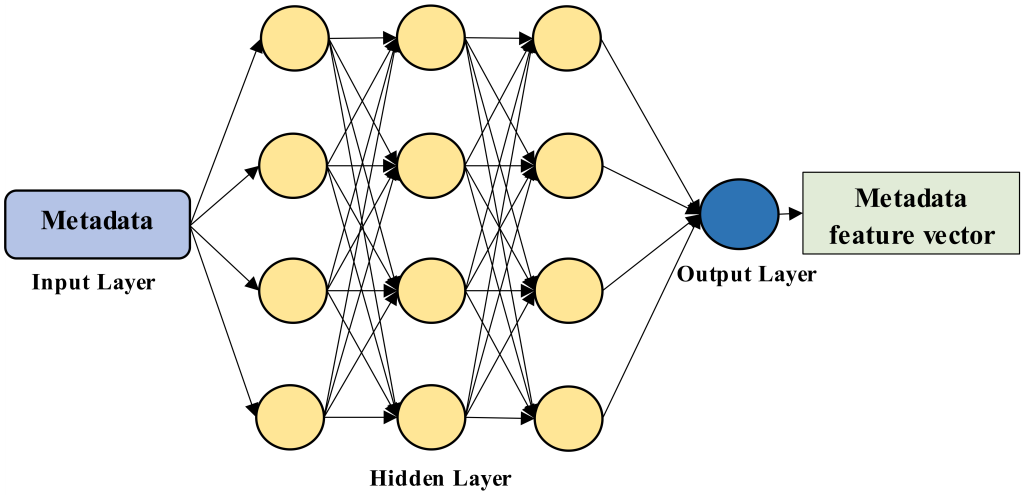


Figure 5. Architecture diagram of the MLP network for feature extraction. The arrows indicate the flow of information between layers of the neural network. The blue block represents the input layer (metadata), yellow circles represent hidden layer neurons, and the blue node represents the output layer. The green block denotes the extracted metadata feature vector.

3.4. Model Training Through Adam Optimizer with ReduceLROnPlateau Scheduler

In this study, we employ the Adam base optimizer [39] with the ReduceLROnPlateau learning rate scheduler [40]. Adam optimizer updates the neural network parameters during training, and the ReduceLROnPlateau scheduler dynamically adjusts the learning rate. The Adam estimates reflect the variations using first m_t and second v_t moment estimations, which are represented in Equations (15) and (16):

$$m_t = \beta_1 m_{t-1} + (1 - \beta_1)\nabla_\theta L_t \tag{15}$$

$$v_t = \beta_2 v_{t-1} + (1 - \beta_2)\left(\nabla_\theta L_t\right)^2 \tag{16}$$

where β_1 and β_2 denote the first and second moment exponential decay parameters, ∇_θ represents the model parameter iteration, and L_t denotes the loss function. These estimates are initialized at zero, and the bias correction is applied to obtain unbiased estimates, as denoted in Equations (17) and (18):

$$\hat{m_t} = \frac{m_t}{1 - \beta_1^t} \tag{17}$$

$$\hat{v_t} = \frac{v_t}{1 - \beta_2^t} \tag{18}$$

The network parameters are updated using the learning rate, as denoted in Equation (19):

$$\theta_{t+1} = \theta_t - \sigma_t \frac{\hat{m_t}}{\sqrt{\hat{v_t}} + \epsilon} \tag{19}$$

where σ_t denotes the learning rate at iteration t and ϵ represents the constant. To achieve convergence stability, the ReduceLROnPlateau scheduler tracks the validation loss during the training process. This will decrease the learning rate every time the performance does not improve after a number of epochs.

The validation loss does not decrease for a patient's period p, and the scheduler reduces the learning rate, as represented in Equation (20):

$$\sigma_{t+1} = \sigma_t * \delta \tag{20}$$

where $\delta \in (0, 1)$ represents the reduction factor. This allows the optimizer to make larger updates during the early training stages. This enables the Adam optimizer with the ReduceLROnPlateau scheduler to reduce the risk of overfitting and improve the model's ability to achieve optimal performance in the IHD classification.

3.5. Gradient-Based Feature Attribution Analysis Using Grad-CAM

In this study, Gradient-weighted Class Activation Mapping (Grad-CAM) is utilized to enhance model interpretability and gradient-based feature attribution analysis. Grad-CAM was adapted to operate on the encoded morphology feature representations generated by the AMDE. For a given input ECG sample, gradients of the predicted class score were computed with respect to the encoded morphology feature vector obtained after the dense encoding layer of the AMDE branch. Each encoded feature corresponds to morphology deviation descriptors extracted from specific ECG waveform regions segmented using the proposed MSEG-R approach. These regions include the P-wave, QRS complex, ST-segment, and T-wave segments across all 12 ECG leads. The importance weight for each encoded feature was estimated using the gradient magnitude, as represented in Equation (21):

$$\alpha_k = \frac{\partial y^c}{\partial z_k} \tag{21}$$

where y^c denotes the predicted score for class c and z_k represents the k-th encoded morphology feature. The resulting attribution scores were projected back onto their corresponding ECG temporal regions according to the morphology segmentation boundaries defined during feature extraction.

4. Results and Discussion

The proposed GAMENet framework was implemented using Python 3.10 with TensorFlow version 1.15 as the deep learning framework. All experiments were conducted on a workstation equipped with an NVIDIA RTX 3080 GPU with 24 GB memory, Intel Core i9

processor, and 64 GB RAM under Ubuntu 22.04 operating system (or your OS). To ensure reproducibility, fixed random seeds were applied for Python, NumPy, TensorFlow, and dataset partitioning operations. The random seed value was set to 42 throughout all experiments. The proposed framework was evaluated using five independent experimental runs, and the final reported performance values correspond to the mean performance across runs.

4.1. Hyperparameter Settings and the Complexity Analysis

The PTB-XL dataset was partitioned using a stratified sample-level split across 70% training, 15% testing, and 15% validation sets. A stratified sample-level partitioning strategy was adopted to preserve the class distribution across the training, validation, and testing subsets. This design minimizes sampling bias and prevents information leakage between subsets. All preprocessing steps, including normalization, filtering, and label encoding, were fitted on the training set and subsequently applied to the validation and test sets using the same parameters.

Model training and hyperparameter tuning were performed using only the training and validation sets, while the test set was held out and used for final performance evaluation. The learning rate was set at 0.001. Typically, the model reaches convergence after approximately 50 epochs. The detailed hyperparameter setting is listed in Table 2.

Table 2. Details of parameter settings.

Components	Parameters	Value
ECG feature extraction	Estimation window	50 samples
	Morphology segments	P, QRS, ST, T
	Deviation features	4
Metadata feature extraction	MLP hidden units	16
	Activation function	ReLU
	Dense layer size	64
	Metadata feature size	16
Prediction layer	Dense units	32
	Dropout rate	0.3
	Output layer	SoftMax
Training parameters	Batch size	32
	Epochs	50
	Loss function	Categorical Cross-Entropy
	Optimizer	Adam
	Learning rate	0.001
	Scheduler	ReduceLROnPlateau

The proposed GAMENet framework includes a dual-branch framework for early IHD classification. The MSEG-R detects R-peaks and segment boundaries in ECG waveforms, and the complexity of the algorithm is found to be $O(N)$. ECG features are computed for each segment (P, QRS, ST, and T), where S denotes the number of segments and L denotes the segment length, with a complexity of $O(SL)$. The metadata feature extractor, through an MLP with input size M, has a complexity of $O(Mh)$. After feature fusion through concatenation, the final classification layer h with k output classes require $O(hk)$ operations. The overall computational complexity of the proposed framework has $O(N + dh + hk)$. This shows the proposed model is effective and suitable for real-time IHD classification using the PTB-XL dataset.

4.2. Performance Analysis of the Proposed GAMENet Framework

This section analyzes the performance metrics of the proposed GAMENet for early IHD classification. The model attains a high reliability of 95.8% accuracy, 95.1% precision, 94.7% recall, specificity of 96.4%, and 94.9% F1-score, indicating strong performance of the proposed model. Also, the MCC of 92%, AUC of 97.2%, and NPV of 95.9% show the strong performance of the proposed model.

The specificity of 96.4% is also high for a very low False Positive Rate (FPR) of 3.6% and a False Negative Rate (FNR) of 3.2% shows minimal misclassification results. Overall, the outcomes prove that the proposed GAMENet provides highly accurate, reliable, and robust prediction of IHD diseases in the early stage.

4.2.1. Model Training Performance

The accuracy and loss graphs deliver a visualization of the learning progress of the proposed GAMENet framework over epochs. The accuracy of the proposed model shows reliable enhancement during the training process. This highlights its adaptability in learning from the PTB-XL dataset. The loss values follow a steady trend, decreasing during the training. This shows the effective convergence of the proposed model for IHD classification, as represented in Figure 6.

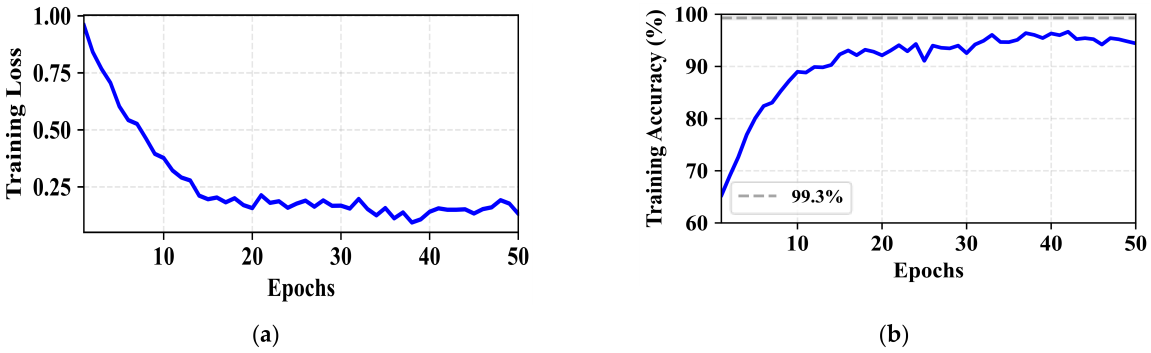


Figure 6. Training and validation (**a**) accuracy and (**b**) loss curves of the proposed GAMENet framework over training epochs.

Figure 7 displays the confusion matrix of the proposed GAMENet framework using three classes, namely normal, early ischemic, and severe ischemic MI. It shows the true positive and true negative classification percentages for each class. Each row denotes the true labels, and each column denotes the predicted labels. This highlights where the model excels and where it struggles in the IHD disease classification task.

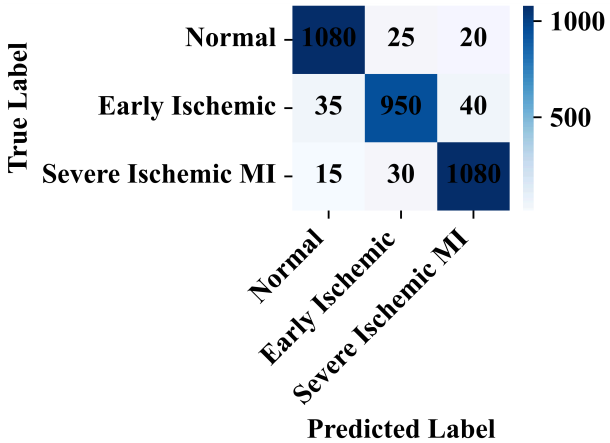


Figure 7. Confusion matrix of the proposed IHD classification framework.

Figure 8 shows the Receiver Operating Characteristic (ROC) curve and its respective AUC values to assess the performance of the proposed model. This marks the true positive rate as opposed to the false positive rate. The values of the AUC range between 0 and 1. Higher values denote higher performance and lower values denote poor performance. It highlights the estimation of how well a model can differentiate between positive and negative rates.

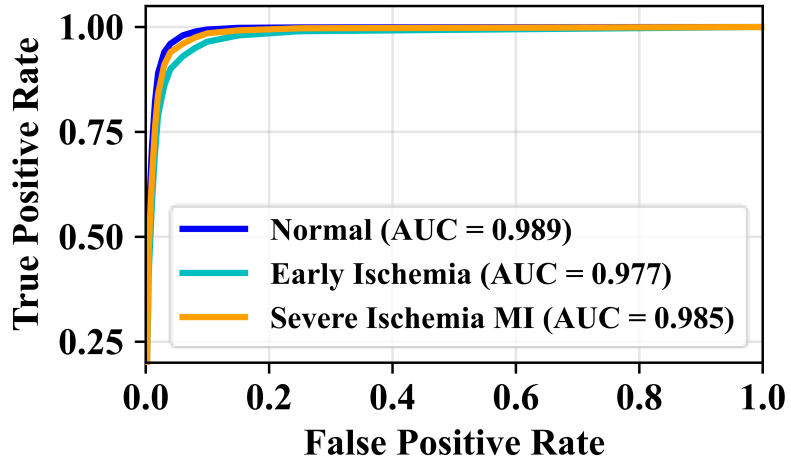


Figure 8. Receiver operating characteristic area under the curve.

Figure 9 shows the AUC curve and its respective precision values to evaluate the performance of the proposed GAMENet framework. This marks the precision value as opposed to the recall value. The values of the precision range between 0 and 1. Higher values denote higher performance and lower values denote poor performance. This highlights the estimation of how well a model can differentiate between positive and negative rates.

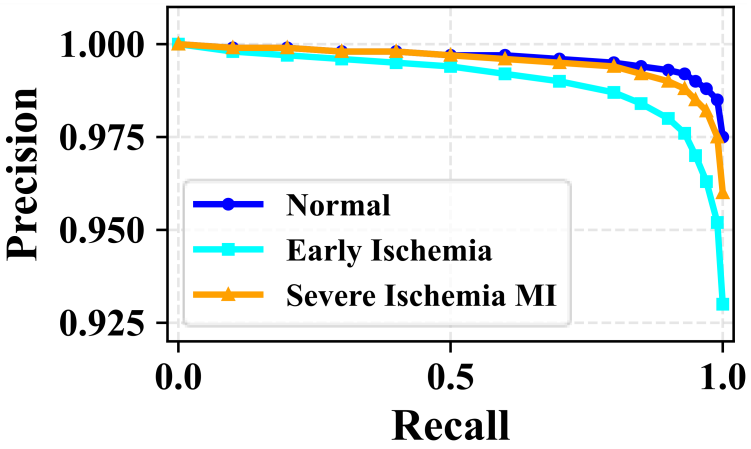


Figure 9. Visualization of the precision-AUC curve.

Figure 10 shows the distribution of metadata of 21,799 ECG records of the PTB-XL dataset. The bars indicate the frequency of records in age groups. The vertical lines show the important statistical indicators: the mean age, median age, and the quartile. As per this graph, male as well as female characteristics are equally represented in the dataset. This visualization represents that both sexes are significantly represented (52% male, and 48% female). This enables the development of a gender-aware ischemia classification framework.

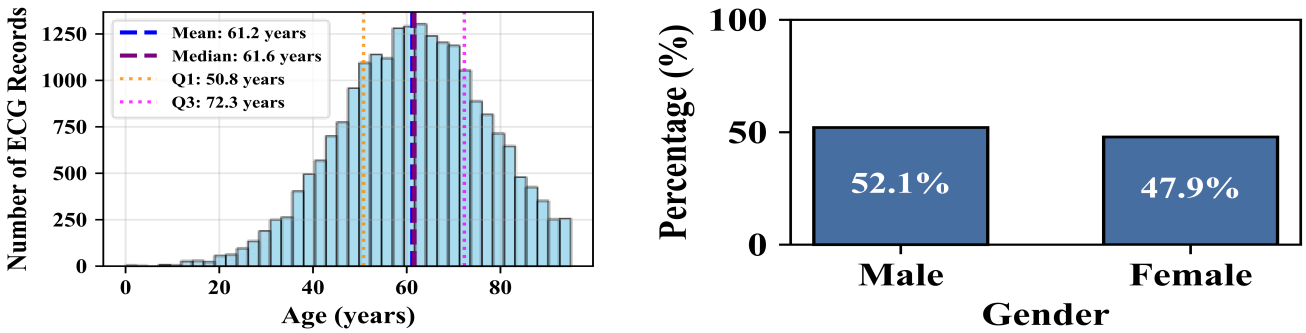


Figure 10. Visualization of the metadata in the PTB-XL dataset.

4.2.2. Performance of the Feature Extraction Phase

Figure 11 shows the cardiac cycle segmentation using R-Peak as an anchor. This figure shows how the detected R-Peak serves as the anchor point for segmenting the complete cardiac cycle. The segmentation enables detailed analysis of each component of the heartbeat. The graph shows each cardiac phase for ischemia detection. The ST-segment shows the detection of early ischemia. The T-wave shows inversion patterns in ischemia. The QRS shows the infarction patterns. Figure 12 shows the cardiac cycle segmentation of the 12-lead ECG signal. This feature extraction process provides the foundation for the GAMENet framework in IHD classification tasks.

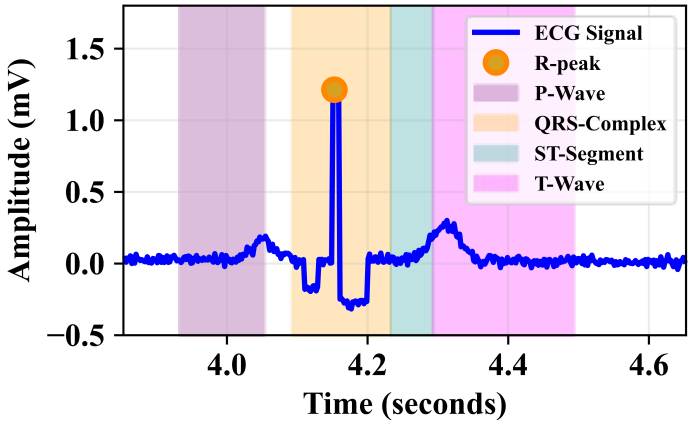


Figure 11. Visualization of ECG morphology-region extraction using R-Peak-anchored temporal windows for P-wave, QRS complex, ST-segment, and T-wave regions.

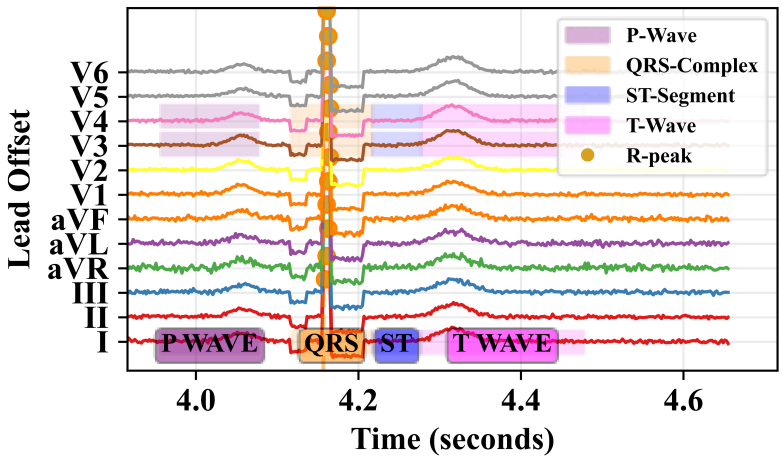


Figure 12. Visualization of 12-lead ECG morphology-region extraction using R-Peak-centered temporal segmentation.

Figure 13 represents the original feature space learned by the proposed model. Each point in the plot corresponds to a patient sample described by the extracted features. T-distributed Stochastic Neighbor Embedding (t-SNE) projects these high-dimensional embeddings onto two axes. This dimensionality reduction shows that the acquired feature representations maintain high discriminative structure. The separation between clusters shows that the model effectively encodes ischemia patterns in the high-dimensional space. This confirms that the proposed feature extraction framework produces a structured and separable embedding space.

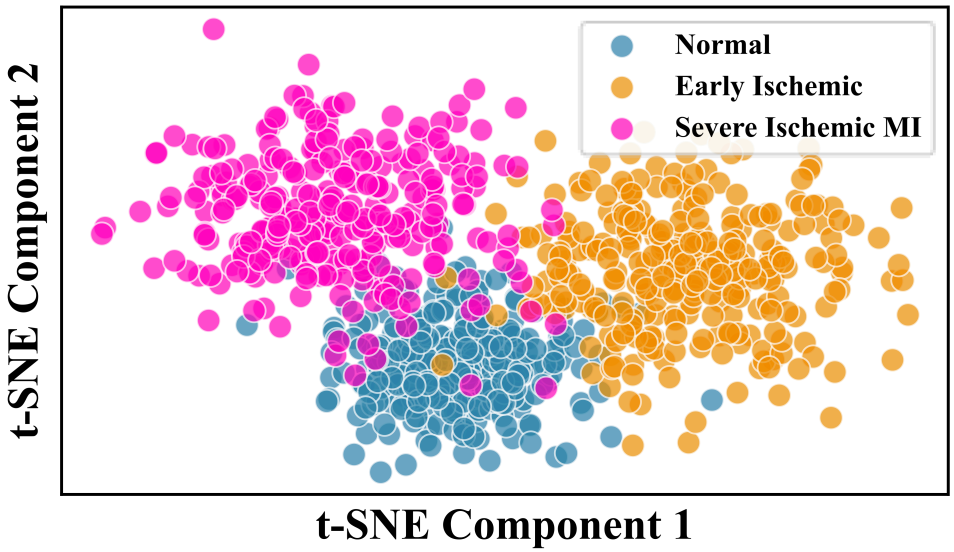


Figure 13. Metadata feature extraction through the MLP.

4.2.3. Gradient-Based Feature Attribution Analysis

Figure 14a shows the normal 12-lead ECG recording from a 45-year-old male patient. The waveform shows regular cardiac cycles with normal morphology. The model should not exhibit strong activation on any particular feature. This uniform low activation confirms that the model differentiates normal from pathological cases. Figure 14b shows a 12-lead ECG recording from a 54-year-old female patient with early ischemic changes. The ECG waveform demonstrates clinically significant abnormalities. The model's focus on T-waves in this female patient confirms that it has learned these gender-specific presentation patterns. The attribution analysis demonstrates that the proposed framework utilizes different morphology regions across sexes. In male ischemic cases, the model highlights ST-segment deviation regions and QRS-related abnormalities associated with myocardial injury. In female patients, the model places greater emphasis on T-wave morphology and diffuse ST-segment changes, which are clinically associated with atypical ischemic presentation and microvascular dysfunction. These observations improve the interpretability of the proposed gender-aware framework and demonstrate consistency with established cardiovascular clinical findings. Figure 14c shows a 12-lead ECG recording from a 62-year-old male patient diagnosed with MI. The ECG waveform shows characteristic cardiac cycles with P-waves, QRS complexes, and T-waves. The Grad-CAM heatmap validates that the model learns clinically relevant patterns. This interpretability shows the model's decision-making process.

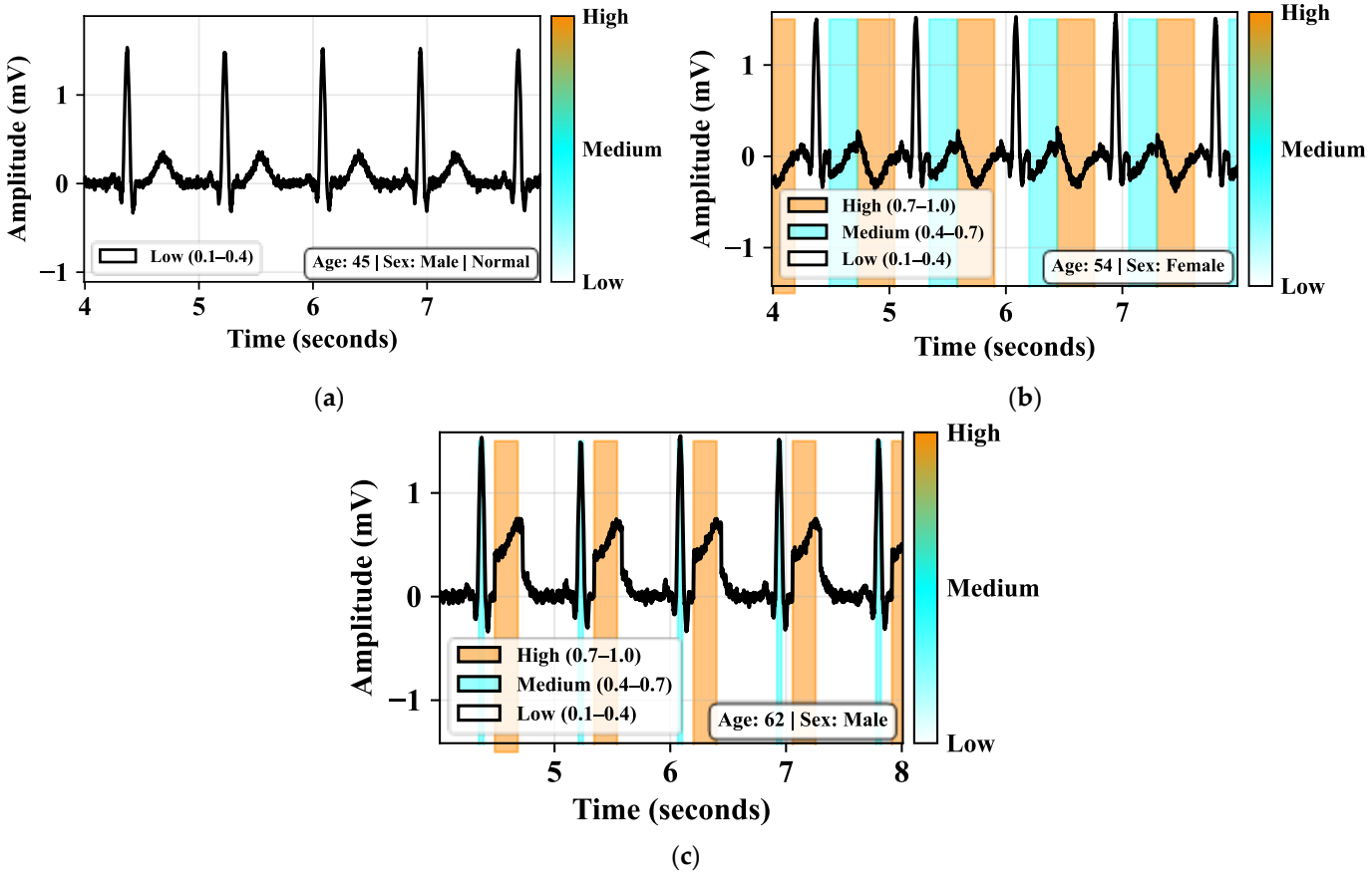


Figure 14. Heatmap visualization of the proposed framework. (**a**) Normal, (**b**) early ischemic condition, and (**c**) severe ischemic MI condition.

4.3. Computational Efficiency Analysis

Table 3 compares the computational complexity of the proposed GAMENet framework with existing models. The proposed GAMENet achieves a minimal inference latency (4.9 ms/sample). This indicates faster performance, also requiring the fewest FLOPs (1.72 GFLOPs) and parameters (4.8 million). This demonstrates that GAMENet is more efficient than all compared models. This ensures the proposed GAMENet offers a balance of speed and resource usage.

Table 3. Computational complexity comparison of the proposed GAMENet framework with baseline architectures.

Model	Inference Time/ECG (ms)	FLOPs (G)	Parameters (Million)	Accuracy (%)
CNN [41]	8.5	2.95	11.8	90.4
CNN + BiLSTM [42]	11.7	2.48	33.2	91.7
ResNet-based ECG Model [43]	14.2	2.10	16.5	92.6
ECG + Metadata Fusion Model [44]	12.4	3.65	14.1	93.4
Proposed GAMENet	4.9	1.72	4.8	95.8

Table 4 presents the mean F1-score (±standard deviation) for each modality-specific model and the proposed GAMENet framework. This shows the performance of the 95% confidence intervals, Wilcoxon test statistics (W), and *p*-values. Results are averaged over multiple runs to ensure reliability, and statistical significance was assessed using the Wilcoxon signed-rank test. The low *p*-values indicate the performance improvements achieved by the proposed GAMENet framework. This supports the robustness and consistency of the proposed approach.

Table 4. Statistical results of the proposed model.

Model	Mean F1-Score ± SD (%)	95% CI (Center)	Test Statistic (W)	*p*-Value
CNN [41]	88.6 ± 1.9	88.6 ± 1.3	18.7	0.012
CNN-BiLSTM [42]	90.8 ± 1.6	90.8 ± 1.1	14.9	0.009
ResNet [43]	92.1 ± 1.4	92.1 ± 0.9	12.6	0.006
Proposed GAMENet	94.9 ± 0.9	94.9 ± 0.6	5.2	0.002

4.4. Cross-Dataset Validation of the Proposed Framework

Table 5 presents the cross-dataset validation performance of the proposed GAMENet framework using multiple publicly available ECG datasets. The experimental results demonstrate that the proposed framework consistently achieves strong classification performance across different ECG data sources. The proposed GAMENet achieved the highest performance on the PTB-XL dataset [45] with 95.8% accuracy, 95.1% precision, 94.7% recall, and 94.9% F1-score. The PTB Diagnostic ECG Database attained 93.14% accuracy and 92.9% F1-score in the proposed framework. This demonstrates effective myocardial infarction classification across dataset size and ECG acquisition characteristics. Similarly, an evaluation on the CPSC 2018 ECG Dataset [46] achieved 94.35% accuracy and 93.73% F1-score. This indicates the strong adaptability across diverse cardiovascular abnormality datasets. The framework also maintained stable performance on the Georgia 12-lead ECG Challenge Dataset [47] with 93.34% accuracy and 92.9% F1-score. To further assess the robustness of the proposed framework, the cross-dataset results were compared with the previously reported results on the same benchmark datasets. Existing studies on the PTB Diagnostic ECG Database have reported classification accuracies generally in the range from 90% to 94% for the detection of myocardial infarction and ischemic heart disease [48,49]. Similarly, the models evaluated on the CPSC 2018 ECG Dataset generally achieve the accuracies above 92% for the classification of ECG abnormalities [50,51]. The performance on the Georgia 12-lead ECG Challenge Dataset decreases due to the inter-patient variability and the acquisition condition differences [52]. Compared with the reported results, the proposed GAMENet framework maintained stable and competitive performance on all the evaluated datasets, with the accuracies of 93.14%, 94.35%, and 93.34% on the PTB Diagnostic ECG Database, CPSC 2018 ECG Dataset, and Georgia 12-lead ECG Challenge Dataset, respectively. The consistent performance across the datasets with different recording protocols and patient populations demonstrates the effectiveness of the morphology-based feature extraction strategy. The incorporation of demographic metadata highlights the generalization capability of the proposed framework. These results show that the proposed GAMENet provides reliable classification performance across heterogeneous ECG datasets.

Table 5. Cross-validation performance analysis of the proposed GAMENet framework.

Datasets	Accuracy (%)	Precision (%)	Recall (%)	F1-Score (%)
PTB Diagnostic ECG Database [45]	93.14	93.21	93.3	92.9
CPSC 2018 ECG Dataset [46]	94.35	93.43	93.43	93.73
Georgia 12-lead ECG Challenge Dataset [47]	93.34	93.22	93.7	92.9
Proposed GAMENet	95.8	95.1	94.7	94.9

4.5. Ablation Study

This section presents the ablation analysis of the proposed GAMENet framework for IHD classification. This analyzes the configuration of the proposed GAMENet framework with different blocks. Table 6 presents the contribution of each component in the proposed GAMENet framework. The results demonstrate that removing any major component leads to a noticeable reduction in classification performance. This confirms the importance of

each module. The complete GAMENet framework achieved the highest performance with 95.8% accuracy and 94.9% F1-score. This confirmed the effectiveness of integrating ECG morphology features, demographic metadata, and optimized training mechanisms for early IHD classification. Table 6 also presents the gender-specific performance analysis of the proposed GAMENet framework.

Table 6. (**a**) Ablation analysis of the proposed GAMENet framework components. (**b**) Gender-specific performance analysis.

(**a**)

Configuration	Accuracy (%)	Precision (%)	Recall (%)	F1-Score (%)
Without ECG preprocessing	90.8	89.9	89.2	89.5
Without metadata preprocessing	91.6	90.7	90.1	90.4
Without gender metadata	93.1	92.1	91.3	91.9
Without AMDE	92.4	91.8	91.2	91.5
Without MSEG-R	93.1	92.4	91.9	92.1
Without MLP	93.6	93.0	92.3	92.6
Without fusion layer	94.2	93.5	92.9	93.2
Without Adam optimizer	92.9	92.1	91.5	91.8
Without ReduceL-ROnPlateau scheduler	94.6	94.0	93.4	93.7
Proposed GAMENet	95.8	95.1	94.7	94.9

(**b**)

Model Configuration	Male				Female			
	Accuracy (%)	Precision (%)	Recall (%)	F1-Score (%)	Accuracy (%)	Precision (%)	Recall (%)	F1-Score (%)
ECG data Only	93.8	93.2	92.6	92.9	89.7	88.9	88.1	88.5
Metadata only	94.6	94.0	93.5	93.7	91.4	90.7	90.1	90.4
ECG + Metadata	96.3	95.8	95.3	95.6	95.1	94.5	93.8	94.2

The results indicate that using only ECG data achieved an accuracy of 93.8% for male patients and 89.7% for female patients. Similarly, the metadata-only configuration produced moderate performance, with accuracies of 94.6% for males and 91.4% for females. The combined ECG + metadata configuration achieved the highest performance for both groups, with accuracies of 96.3% for male patients and 95.1% for female patients. These demonstrate that integrating ECG morphology features with demographic metadata significantly enhances classification performance and helps the framework capture sex-specific variations in IHD presentation.

4.6. Comparative Analysis

Table 7 compares the proposed GAMENet with the existing state-of-the-art approaches. The existing ML with discrete wavelet transforms, AlexNet50 with fuzzy bi-clustering, RF and XGBoost, GKVDLNN, and RABFN attained an accuracy of 92%, 89%, 95.45%, 94.89%, and 94.24%, respectively. Existing approaches achieved a lower classification accuracy compared to the proposed GAMENet framework. The proposed GAMENet framework provides several practical advantages for ischemic heart disease classification. Unlike existing approaches, GAMENet integrates ECG morphology features with demographic metadata to enable gender-aware learning and improve classification robustness across male and female patient groups. The proposed framework performs interpretable morphology-region analysis using P-wave, QRS complex, ST-segment, and T-wave segmentation. The proposed framework obtains an accuracy of 95.8%, a precision of 95.1%, a recall of 94.7%, an F1-score of 94.9%, and a specificity of 96.4%. The table demonstrates that the proposed GAMENet framework achieves improved detection performance compared to recent ischemia detection approaches with the same PTB-XL datasets and the same processing pipeline. This ensures the fairness of the proposed framework in IHD classification. These

characteristics make the proposed framework more suitable for clinically interpretable and real-time ECG-based IHD diagnosis.

Table 7. Comparative analysis with state-of-the-art approaches.

Reference	Model	Accuracy (%)	Precision (%)	Recall (%)	F1-Score (%)	Specificity (%)
Suhail et al. 2022 [17]	ML with discrete wavelet transform	92	94	83	83	88
Iqbal, 2024 [18]	AlexNet50 with fuzzy bi-clustering	89	88.90	88.70	88.80	88.76
Majhi and Kashyap, 2024 [19]	RF and XGBoost	95.45	94.73	94.73	94.73	96
Jyothi and Padeepini, 2024 [20]	GKVDLNN	94.89	88.96	86.36	86.36	93.4
Rath et al. 2022 [21]	RABFN	94.24	94.2	92.0	94.2	94.23
Proposed	GAMENet	95.8	95.1	94.7	94.9	96.4

4.7. Discussion

The proposed GAMENet addressed several limitations in traditional ECG-based IHD detection models. In this study, the proposed framework integrated AMDE features extracted from ECG segments with patient demographic metadata to improve early detection of ischemic conditions. The inclusion of the encoder network was important because ischemic ECG morphology deviations frequently exhibit nonlinear interdependencies across waveform regions and leads. Although handcrafted morphology descriptors provide interpretable clinical information, direct classification of the raw extracted features may not sufficiently capture subtle latent relationships associated with early ischemic progression. The encoder improves representation compactness, feature interaction modeling, and demographic-aware fusion while preserving clinically meaningful morphology characteristics. Traditional DL models depend on automatic feature extraction from raw ECG signals. However, existing approaches require large training datasets and struggle to capture subtle morphological deviations associated with early IHD. The proposed GAMENet models ECG morphology by computing deviation features from physiologically meaningful segments. This structured feature extraction method enables the model to focus on clinically relevant waveform characteristics. The proposed GAMENet segments the ECG signal using MSEG-R. The proposed MSEG-R framework utilizes R-peak-centered temporal segmentation to isolate clinically relevant ECG morphology regions. The R-Peak was used as a stable temporal anchor for heartbeat alignment, while predefined temporal windows were employed to approximate the P-wave, QRS complex, ST-segment, and T-wave regions. This approach was designed to enable robust morphology-based feature extraction while maintaining computational efficiency for large-scale ECG analysis. The proposed framework aligns the waveform segments relative to the R-peak. The model ensures consistent extraction of the P-wave, QRS complex, ST-segment, and T-wave across all samples. This segmentation-based approach allows for the computation of multiple deviation features, including mean deviation, maximum deviation, slope deviation, and area deviation. This provided a detailed representation of ECG morphology.

The performance of the proposed model was evaluated using the PTB-XL dataset and compared with several DL approaches. The proposed GAMENet utilizes a compact feature representation based on morphology deviation encoding. This significantly reduces the dimensionality of the feature space before classification. This ensures the model maintains high classification accuracy while remaining computationally efficient. The proposed model is the integration of demographic metadata into the classification framework. Most existing ECG classification models depend on physiological signals and ignore patient-specific characteristics. An important advantage of the proposed framework is its ability to model sex-specific ECG morphology variations associated with IHD. Clinical studies report that men commonly exhibit more localized ST-segment elevation/depression and

infarction-related QRS abnormalities, whereas women often present with subtler ischemic manifestations such as diffuse ST-T abnormalities, T-wave inversion, and non-specific repolarization changes. These atypical ECG presentations in women frequently contribute to underdiagnosis and delayed clinical intervention. By integrating morphology-aware ECG segmentation with demographic metadata, the proposed GAMENet framework is able to capture these sex-dependent electrophysiological patterns, thereby improving both classification performance and clinical interpretability.

The comparative analysis presented demonstrates that the proposed GAMENet achieves competitive and consistently strong performance across all evaluation metrics. These results indicate that the integration of morphology-aware ECG feature extraction and demographic metadata contributes to improved classification performance while maintaining clinical interpretability. In addition to quantitative performance gains, the proposed framework provides gender-aware analysis and morphology-region interpretability. The improvement is particularly notable in the detection of early ischemic cases. Another important advantage of the proposed method is its interpretability. This interpretability is valuable in clinical settings. These transparent decision-making processes are essential for ensuring reliable diagnosis. The comparative analysis demonstrates that the proposed GAMENet framework offers several advantages over existing ECG classification approaches. The combination of morphology-based feature extraction with demographic metadata integration enables improved diagnostic accuracy and interpretability. The experimental results confirm that the proposed framework provides a robust solution for automated IHD classification. This provides a promising tool for supporting clinical decision-making in cardiovascular healthcare systems. To evaluate the clinical relevance of the attribution maps, the highlighted ECG regions were compared against clinically recognized ischemic biomarkers described in cardiology literature, including ST-segment deviation, T-wave inversion, and QRS abnormalities associated with myocardial injury. The attribution analysis consistently emphasized these waveform regions in ischemic and severe MI cases. In female ECG recordings, stronger activations were frequently observed in diffuse ST-T abnormality regions, whereas male ECG recordings demonstrated more localized ST-segment and QRS-related activations. These observations are consistent with established clinical findings regarding sex-specific ischemic ECG presentation patterns. An important aspect of the proposed framework is the sex-stratified evaluation performed for male and female patient groups. Experimental results demonstrated that ECG-only classification produced a noticeable performance gap between sexes, with lower classification accuracy observed in female patients. This observation is consistent with clinical evidence showing that women frequently present with atypical or subtle ischemic ECG compared to men. After integrating demographic metadata with morphology-based ECG features, the proposed GAMENet framework reduced the performance disparity and improved classification robustness across both sexes. These findings support the effectiveness of the gender-aware architecture and highlight the importance of incorporating demographic context in automated IHD diagnosis systems.

However, the study faces some limitations. The proposed framework is evaluated on the PTB-XL dataset, which does not represent the diversity of real-world clinical populations. The segmentation process using R-Peak anchoring is sensitive to noisy ECG signals. Furthermore, the ECG-based diagnosis fails to detect certain ischemic conditions such as non-obstructive coronary artery disease or microvascular ischemia, which are more prevalent in women. Also, the proposed framework focuses on the classification of ischemic stages that fail to predict long-term patient outcomes. In the future, we will expand the proposed framework to address these problems. Future work was validated on multi-center clinical datasets to improve generalizability across different patient popula-

tions. The longitudinal prediction models that analyze sequential ECG recordings to detect early disease progression and the prediction of adverse cardiac events can be performed in the future. This enables proactive clinical intervention and personalized IHD support.

5. Conclusions

The study successfully developed a GAMENet framework for early IHD detection. The proposed framework integrated ECG morphology deviation features extracted through the AMDE with metadata features extracted through MLP. The proposed GAMENet framework analyzes ECG signals and demographic information for identifying three clinical conditions: normal, early ischemic, and severe ischemic MI. The framework utilized ECG preprocessing and segmentation through MSEG-R to isolate clinically significant waveform segments, including the P-wave, QRS complex, ST-segment, and T-wave. The extracted ECG and metadata features were fused and used for final classification. Experimental evaluation conducted on the PTB-XL dataset demonstrated that the proposed model achieved an accuracy of 95.8%, precision of 95.1%, recall of 94.7%, and an F1-score of 94.9%. The cross-dataset validation and ablation studies further confirmed the robustness and effectiveness of the morphology-based feature extraction and gender-aware metadata integration strategies. These findings support the suitability of the proposed framework for interpretable and reliable ischemic heart disease classification. The results confirm that incorporating morphology-based ECG feature extraction with metadata significantly enhances diagnostic performance while maintaining computational efficiency and interpretability. The proposed approach provides a reliable and scalable solution for supporting cardiovascular diagnosis and assists clinicians in early IHD detection and clinical decision-making.

Author Contributions: All authors contributed to the conception of the problem setting and overall design of the work. D.C. built the conceptualization and methodology. A.D. implemented the work and writing. All authors were involved in the visualization of concepts. This version was revised and improved by all authors. All authors have read and agreed to the published version of the manuscript.

Funding: This research received no external funding.

Institutional Review Board Statement: Not applicable.

Informed Consent Statement: Not applicable.

Data Availability Statement: The data presented in this study are openly available in https://physionet.org/content/ptb-xl/1.0.3/ (accessed on 15 February 2026).

Conflicts of Interest: The authors declare no conflicts of interest.

References

1. Heusch, G. Myocardial ischemia/reperfusion: Translational pathophysiology of ischemic heart disease. *Med* **2024**, *5*, 10–31. [CrossRef] [PubMed]
2. Schindler, T.H.; Arai, A.E.; Berry, C.; Sykes, R.; Nieman, K.; Kitagawa, K.; Chandrashekhar, Y.; Li, S.; Xie, F.; Porter, T.R.; et al. Myocardial blood flow assessment and reporting for ischemic heart disease: Cardiac PET, MR, CT, and echocardiography. *Cardiovasc. Imaging* **2026**, *19*, 378–411.
3. Ding, Y.; Deng, A.; Qi, T.F.; Yu, H.; Wu, L.P.; Zhang, H. The burden and trend prediction of ischemic heart disease associated with lead exposure: Insights from the Global Burden of Disease study 2021. *Environ. Health* **2025**, *24*, 23. [CrossRef] [PubMed]
4. Jabeen, S.; Bibi, M.; Shah, S.; Ali, A.A.; Bahloul, M.A. Data-driven based approaches for early diagnosis of Ischemic Heart Disease (IHD): A review of recent advancements, challenges, and opportunities. *Biomed. Signal Process. Control* **2026**, *113*, 108816.
5. Saito, Y.; Tateishi, K.; Kato, K.; Kitahara, H.; Kobayashi, Y. Standard and non-standard cardiovascular risk factors in ischemic heart disease and atherosclerotic cardiovascular disease: A clinical review. *Intern. Med.* **2026**, *65*, 508–519. [CrossRef] [PubMed]
6. Rodriguez Lozano, P.F.; Rrapo Kaso, E.; Bourque, J.M.; Morsy, M.; Taylor, A.M.; Villines, T.C.; Kramer, C.M.; Salerno, M. Cardiovascular imaging for ischemic heart disease in women: Time for a paradigm shift. *Cardiovasc. Imaging* **2022**, *15*, 1488–1501.

7. Dziedzic, E.A.; Gąsior, J.S.; Tuzimek, A.; Kochman, W. Blood count-derived inflammatory markers and acute complications of ischemic heart disease in elderly women. *J. Clin. Med.* **2023**, *12*, 1369. [CrossRef] [PubMed]
8. Niu, Y.; Wang, G.; Feng, X.; Niu, H.; Shi, W. Significance of fatty liver index to detect prevalent ischemic heart disease: Evidence from national health and nutrition examination survey 1999–2016. *Front. Cardiovasc. Med.* **2023**, *10*, 1171754. [CrossRef] [PubMed]
9. Deepti, C.; Nagaraja, J. Cardio vascular disease prediction by deep learning based on IOMT: Review. *Diagnostics* **2024**, *16*, 161.
10. Hangaragi, S.; Neelima, N.; Jegdic, K.; Nagarwal, A. Integrated fusion approach for multi-class heart disease classification through ECG and PCG signals with deep hybrid neural networks. *Sci. Rep.* **2025**, *15*, 8129. [CrossRef] [PubMed]
11. Marzoog, B.A.; Chomakhidze, P.; Gognieva, D.; Silantyev, A.; Suvorov, A.; Abdullaev, M.; Mozzhukhina, N.; Filippova, D.A.; Kostin, S.V.; Kolpashnikova, M.; et al. Development and validation of a machine learning model for diagnosis of ischemic heart disease using single-lead electrocardiogram parameters. *World J. Cardiol.* **2025**, *17*, 104396. [CrossRef] [PubMed]
12. Butler, L.; Ivanov, A.; Celik, T.; Karabayir, I.; Chinthala, L.; Hudson, M.M.; Ness, K.K.; Mulrooney, D.A.; Dixon, S.B.; Tootooni, M.S.; et al. Feasibility of remote monitoring for fatal coronary heart disease using Apple Watch ECGs. *Cardiovasc. Digit. Health J.* **2024**, *5*, 115–121. [CrossRef] [PubMed]
13. Saffar Soflaei, S.; Abedsaeidi, M.; Nazar, E.; Varasteh, N.; Kooshki, A.; Moodi Ghalibaf, A.; Farsi, F.; Esmaily, H.; Moohebati, M.; Ferns, G.A.; et al. Predictive Value of ECG Ischemic Pattern Changes for the 10-Year Occurrence of Ischemic Heart Disease. *Ann. Noninvasive Electrocardiol.* **2025**, *30*, e70111. [CrossRef] [PubMed]
14. Malakouti, S.M. Heart disease classification based on ECG using machine learning models. *Biomed. Signal Process. Control* **2023**, *84*, 104796. [CrossRef]
15. Karthik, S.; Santhosh, M.; Kavitha, M.S.; Paul, A.C. Automated Deep Learning Based Cardiovascular Disease Diagnosis Using ECG Signals. *Comput. Syst. Sci. Eng.* **2022**, *42*, 183–199. [CrossRef]
16. Golande, A.L.; Pavankumar, T. Optical electrocardiogram-based heart disease prediction using hybrid deep learning. *J. Big Data* **2023**, *10*, 139.
17. Suhail, M.M.; Razak, T.A. Cardiac disease detection from ECG signal using discrete wavelet transform with machine learning method. *Diabetes Res. Clin. Pract.* **2022**, *187*, 109852. [CrossRef] [PubMed]
18. Iqbal, J.M. A novel deep learning approach for early detection of cardiovascular diseases from ECG signals. *Med. Eng. Phys.* **2024**, *125*, 104111. [CrossRef] [PubMed]
19. Majhi, B.; Kashyap, A. Explainable AI-driven machine learning for heart disease detection using ECG signal. *Appl. Soft Comput.* **2024**, *167*, 112225. [CrossRef]
20. Jyothi, P.; Pradeepini, G. Heart disease detection system based on ECG and PCG signals with the aid of GKVDLNN classifier. *Multimed. Tools Appl.* **2024**, *83*, 30587–30612.
21. Rath, A.; Mishra, D.; Panda, G.; Satapathy, S.C.; Xia, K. Improved heart disease detection from ECG signal using deep learning-based ensemble model. *Sustain. Comput. Inform. Syst.* **2022**, *35*, 100732.
22. Abdullayev, I.N.; Jiyanbayev, O.E.; Nasimov, R.K. Early Detection and Prognostic Assessment of Ischemic Heart Diseases Based on Multimodal Artificial Intelligence Algorithms. *Tech. Sci. Integr. Res.* **2026**, *2*, 33–42.
23. Her, A.Y.; Dischl, D.; Kim, Y.H.; Kim, S.W.; Shin, E.S. Magnetocardiography for the detection of myocardial ischemia. *Front. Cardiovasc. Med.* **2023**, *10*, 1242215. [CrossRef] [PubMed]
24. Stone, P.H.; Libby, P.; Boden, W.E. Fundamental pathobiology of coronary atherosclerosis and clinical implications for chronic ischemic heart disease management—The plaque hypothesis: A narrative review. *JAMA Cardiol.* **2023**, *8*, 192–201. [PubMed]
25. Zhang, Z.; Dalan, R.; Hu, Z.; Wang, J.W.; Chew, N.W.; Poh, K.K.; Tan, R.S.; Soong, T.W.; Dai, Y.; Ye, L.; et al. Reactive oxygen species scavenging nanomedicine for the treatment of ischemic heart disease. *Adv. Mater.* **2022**, *34*, 2202169. [CrossRef] [PubMed]
26. Razo, C.; Welgan, C.A.; Johnson, C.O.; McLaughlin, S.A.; Iannucci, V.; Rodgers, A.; Wang, N.; LeGrand, K.E.; Sorensen, R.J.; He, J.; et al. Effects of elevated systolic blood pressure on ischemic heart disease: A Burden of Proof study. *Nat. Med.* **2022**, *28*, 2056–2065. [CrossRef] [PubMed]
27. Alfa, M.; Samann, F.; Schanze, T. ML-CDAE: Multi-Lead Convolutional Denoising Autoencoder for Denoising 12-Lead ECG Signals. *Signals* **2026**, *7*, 18. [CrossRef]
28. Pachiyannan, P.; Alsulami, M.; Alsadie, D.; Saudagar, A.K.J.; AlKhathami, M.; Poonia, R.C. A novel machine learning-based prediction method for early detection and diagnosis of congenital heart disease using ECG signal processing. *Technologies* **2024**, *12*, 4. [CrossRef]
29. Jandera, A.; Petryk, Y.; Muzelak, M.; Skovranek, T. ECG Signal Analysis and Abnormality Detection Application. *Algorithms* **2025**, *18*, 689. [CrossRef]
30. Rath, A.; Mishra, D.; Panda, G. Imbalanced ECG signal-based heart disease classification using ensemble machine learning technique. *Front. Big Data* **2022**, *5*, 1021518. [CrossRef] [PubMed]
31. PTB-XL Dataset Link. Available online: https://physionet.org/content/ptb-xl/1.0.3/ (accessed on 15 February 2026).
32. Oancea, V.; Kung, Y.L.; Murphy, J.R.; Piraino, P.; Given, J.W. Waveforms from nuclear explosions (WFNE) repository. *Pure Appl. Geophys.* **2024**, *182*, 5109–5127. [CrossRef]

33. Krishna, N.; Padmasine, K.G. A review on microwave band pass filters: Materials and design optimization techniques for wireless communication systems. *Mater. Sci. Semicond. Process.* **2023**, *154*, 107181.
34. Geem, D.; Hercules, D.; Pelia, R.S.; Venkateswaran, S.; Griffiths, A.; Noe, J.D.; Dotson, J.L.; Snapper, S.; Rabizadeh, S.; Rosh, J.R.; et al. Progression of pediatric Crohn's disease is associated with anti–tumor necrosis factor timing and body mass index Z-score normalization. *Clin. Gastroenterol. Hepatol.* **2024**, *22*, 368–376. [PubMed]
35. Herdian, C.; Kamila, A.; Budidarma, I.G.A.M. Studi Kasus Feature Engineering Untuk Data Teks: Perbandingan Label Encoding dan One-Hot Encoding Pada Metode Linear Regresi. *Technol. J. Ilm.* **2024**, *15*, 93–108. [CrossRef]
36. Permatahati, I.; Muqorobin, M. Computer sales forecasting system application using web-based single moving average method. *Int. J. Comput. Inf. Syst.* **2022**, *3*, 56–63. [CrossRef]
37. Hu, M.; Yi, H.; Yan, W.; Ren, W.; Wang, J.; Qi, F. Multi-site cardiac rhythm monitoring via multi-channel SCG system and exercise-induced physiological analysis. *Front. Physiol.* **2026**, *17*, 1727160. [CrossRef] [PubMed]
38. Afzal, S.; Ziapour, B.M.; Shokri, A.; Shakibi, H.; Sobhani, B. Building energy consumption prediction using multilayer perceptron neural network-assisted models; comparison of different optimization algorithms. *Energy* **2023**, *282*, 128446. [CrossRef]
39. Liu, M.; Yao, D.; Liu, Z.; Guo, J.; Chen, J. An improved Adam optimization algorithm combining adaptive coefficients and composite gradients based on randomized block coordinate descent. *Comput. Intell. Neurosci.* **2023**, *2023*, 4765891. [CrossRef] [PubMed]
40. Thakur, A.; Gupta, M.; Sinha, D.K.; Mishra, K.K.; Venkatesan, V.K.; Guluwadi, S. Transformative breast Cancer diagnosis using CNNs with optimized ReduceLROnPlateau and Early stopping Enhancements. *Int. J. Comput. Intell. Syst.* **2024**, *17*, 14.
41. Jain, A.; Rao, A.C.S.; Jain, P.K.; Hu, Y.C. Optimized levy flight model for heart disease prediction using CNN framework in big data application. *Expert Syst. Appl.* **2023**, *223*, 119859. [CrossRef]
42. Pandey, V.; Lilhore, U.K.; Walia, R.; Alroobaea, R.; Alsafyani, M.; Baqasah, A.M.; Algarni, S. Enhancing heart disease classification with M2MASC and CNN-BiLSTM integration for improved accuracy. *Sci. Rep.* **2024**, *14*, 24221. [CrossRef] [PubMed]
43. Kumar, S.S.; Rinku, D.R.; Kumar, A.P.; Maddula, R.; Palagan, C.A. An IOT framework for detecting cardiac arrhythmias in real-time using deep learning resnet model. *Meas. Sens.* **2023**, *29*, 100866. [CrossRef]
44. Nakanishi, R.; Hirata, A.; Kubota, Y. Deep Learning-Based Multi-Lead ECG Reconstruction from Lead I with Metadata Integration and Uncertainty Estimation. *Sensors* **2025**, *26*, 212. [PubMed]
45. PTB Diagnostic ECG Database Link. Available online: https://www.physionet.org/content/ptbdb/1.0.0/ (accessed on 15 February 2026).
46. CPSC 2018 ECG Dataset Link. Available online: https://physionet.org/content/challenge-2020/1.0.2/papers/ (accessed on 15 February 2026).
47. Georgia 12-Lead ECG Challenge Dataset Link. Available online: https://www.kaggle.com/datasets/physionet/georgia-12lead-ecg-challenge-database (accessed on 15 February 2026).
48. Airlangga, G. Enhancing cardiac anomaly detection through deep learning autoencoder: An in-depth analysis using the PTB diagnostic ECG database. *G-Tech J. Teknol. Terap.* **2024**, *8*, 584–592.
49. Darghaoth, A. Comparative Evaluation of Deep Learning Models for ECG Classification Using MIT-BIH and PTB Datasets. *J. Methodical Comput. Commun.* **2025**, *2025*, 41–53.
50. Dhyani, S.; Kumar, A.; Choudhury, S. Analysis of ECG-based arrhythmia detection system using machine learning. *MethodsX* **2023**, *10*, 102195. [CrossRef] [PubMed]
51. Zhang, H.; Gu, H.; Gao, J.; Lu, P.; Chen, G.; Wang, Z. An effective atrial fibrillation detection from short single-lead electrocardiogram recordings using MCNN-BLSTM network. *Algorithms* **2022**, *15*, 454.
52. Perez Alday, E.A.; Gu, A.; Shah, A.J.; Robichaux, C.; Ian Wong, A.K.; Liu, C.; Liu, F.; Bahrami Rad, A.; Elola, A.; Seyedi, S.; et al. Classification of 12-lead ecgs: The physionet/computing in cardiology challenge 2020. *Physiol. Meas.* **2020**, *41*, 124003. [CrossRef] [PubMed]

Disclaimer/Publisher's Note: The statements, opinions and data contained in all publications are solely those of the individual author(s) and contributor(s) and not of MDPI and/or the editor(s). MDPI and/or the editor(s) disclaim responsibility for any injury to people or property resulting from any ideas, methods, instructions or products referred to in the content.